

# Improper s-wave symmetry for the electronic pairing in iron-based superconductors by first-principles calculations

M. Casula\*

CNRS and Institut de Minéralogie et de Physique des Milieux condensés,  
Université Pierre et Marie Curie, case 115, 4 place Jussieu, 75252, Paris cedex 05, France

S. Sorella†

International School for Advanced Studies (SISSA) Via Beirut 2,4 34014 Trieste,  
Italy and INFN Democritos National Simulation Center, Trieste, Italy

(Dated: September 15, 2021)

By means of space-group symmetry arguments, we argue that the electronic pairing in iron-based high temperature superconductors shows a structure which is a linear combination of *planar* s-wave and d-wave symmetry channels, both preserving the 3-dimensional  $A_{1g}$  irreducible representation of the corresponding crystal point-group. We demonstrate that the s- and d-wave channels are determined by the parity under reflection of the electronic orbitals through the iron planes, and by improper rotations around the iron sites. We provide evidence of these general properties by performing accurate quantum Monte Carlo ab-initio calculations of the pairing function, for a FeSe lattice with tetragonal experimental geometry at ambient pressure. We find that this picture survives even in the FeSe under pressure and at low temperatures, when the tetragonal point-group symmetry is slightly broken. In order to achieve a higher resolution in momentum space we introduce a BCS model that faithfully describes our QMC variational pairing function on the simulated 4x4 FeSe unit cell. This allows us to provide a k-resolved image of the pairing function, and show that non-isotropic contributions in the BCS gap function are related to the improper s-wave symmetry. Our theory can rationalize and explain a series of contradictory experimental findings, such as the observation of twofold symmetry in the FeSe superconducting phase, the anomalous drop of  $T_c$  with Co-impurity in  $\text{LaFeAsO}_{(1-x)}\text{F}_x$ , the s-to-d-wave gap transition in  $\text{BaFe}_2\text{As}_2$  under K doping, and the nodes appearing in the  $\text{LiFeAs}$  superconducting gap upon P isovalent substitution.

PACS numbers: 74.20.-z, 74.20.Mn, 74.70.Xa, 02.70.Ss

## I. INTRODUCTION

The pairing symmetry of the superconducting state in iron-based superconductors (IBS) has been one of the most debated subjects since their first discovery, in both theory and experiments.<sup>1,3,4</sup> Its determination is particularly challenging in the IBS for their complex electronic structure, with a strong multiband character, and a Fermi surface constituted by many sheets, which can vary with doping and chemical composition. Moreover, the IBS families are usually compensated metals, and thus both electrons and holes are involved in the paired state. Weak-coupling RPA approaches, coupled to multiband BCS theory, yield a pairing function with global s-wave ( $A_{1g}$ ) symmetry, but with electron and holes pockets having opposite sign. This scenario, dubbed  $s^\pm$ , was first proposed by Mazin *et al.*<sup>5</sup> complemented later with its variants, called “extended  $s^\pm$ ”,<sup>6</sup> in the case that accidental nodes appear on a single Fermi sheet without breaking the full rotational symmetry. The latest generalizations include also “weak” nodal lines which develop as closed loops on the 3-dimensional (3D) Fermi surface.<sup>7-9</sup>

A variety of experiments has been performed to probe the pairing symmetry of IBS, ranging from thermal conductivity and specific heat measurements to angle-resolved photoemission spectroscopy. While there is no doubt on the spin singlet nature of the pairing state as revealed by the Knight shift,<sup>10</sup> the presence of nodes and the total symmetry of the spatial part of the pairing function are controversial. In fact, the experimental outcome seems to lack universality, as it depends crucially

on the “family” of tested compound, its doping, its isovalent substitutions, and its level of disorder. For instance, the situation is paradoxical for the “111” family, where the  $\text{LiFeAs}$  material shows a fully gapped superconducting order parameter, while the isovalent substitution of arsenic by phosphorus leads to thermodynamic properties compatible with a nodal pairing function.<sup>11</sup> For the “122” family, there is a recent claim, supported by independent experimental probes, that the pairing in the  $\text{BaFe}_2\text{As}_2$  undergoes an s-to-d symmetry change by doping with potassium,<sup>12</sup> the fully substituted  $\text{KFe}_2\text{As}_2$  being identified as a d-wave superconductor.<sup>13</sup> In the “1111” family, the dependence of the critical temperature  $T_c$  upon disorder has been studied in the  $\text{LaFeAsO}_{(1-x)}\text{F}_x$  with  $x = 0.11$ . It has been found that Co-doping induced disorder makes  $T_c$  to fall much more slowly than Mn-doping.<sup>14</sup> This is certainly not compatible with a doping independent pairing function with sign changes (either  $s^\pm$  or d-wave).

Finally, specific heat measurements performed on the FeSe revealed a highly anisotropic order parameter in the “11” family,<sup>15</sup> with a twofold symmetry directly observed by scanning tunneling microscopy (STM).<sup>16</sup>

In this paper, we study the IBS gap structure from a different perspective, namely by looking for its *universal* features based on symmetry constraints induced by the 3D *space-group* transformations of the crystals. We prove that the IBS pairing function is a linear combination of terms having planar s- and d-wave symmetries, both fulfilling the full 3D  $A_{1g}$  representation. These properties are then verified in the FeSe by performing state-of-the-art quantum Monte Carlo (QMC) calculations from first-principles. Our theory provides a gen-

eral framework to account for the contradictory experimental outcomes.

The paper is organized as it follows. In Sec. II we present the derivation of the 2D iron lattice model consistent with the symmetries of the 3D point group of the FeSe. We show that it is necessary to include improper rotations and a gauge transformation for translations in order to define a 2D square lattice model consistent with the 3D structure. We study what are the implications of the symmetry constraints for the pairing structure, and show that a  $d_{xy}$ -wave channel is present beside the extended s-wave one. These predictions are verified by accurate quantum Monte Carlo simulations, presented in Sec. III, to determine the global symmetry of the pairing function from first-principles. In Sec. IV we model the ab-initio pairing function by means of a BCS Hamiltonian. This allows us to compute the BCS gap on a dense k-point grid, and study its nodal structure in the k-space. In Sec. V we relate our findings to the experimental outcome in FeSe, and to other experiments in different families of iron pnictides and chalcogenides.

## II. IMPROPER $S_4$ SYMMETRY

The undistorted structure of FeSe, together with the other parent compounds of the “111” and “1111” families, belongs to the  $P4/nmm$  space-group, which is nonsymmorphic due to a glide plane parallel to the iron layers. Indeed, its related  $D_{4h}$  point-group classes contain certain operations with the nonprimitive lattice translation  $\tau = (1/2, 1/2, 0)$  - expressed in crystal units of the 2-Fe unit cell - which brings a Fe site into the other in the cell. This is due to the Se sites alternating above and below the Fe layer (see Fig.1).

In particular, the  $C_4$  subgroup generated by pure rotations by  $\pi/2$  about the principal axis is not compatible with the structure of the solid. On the other hand, the  $S_4$  subgroup, defined with the rotation by  $\pi/2$  about the principal axis combined with the reflection  $\sigma_h$  through the Fe plane ( $S_4 = C_4\sigma_h$ ), is a pure point-group operation allowed by the  $P4/nmm$  space-group, as well as the reflection through the plane perpendicular to the Fe (xy) plane and bisecting the secondary (x and y) axes (the  $\sigma_d$  element).<sup>2</sup>

This has important consequences on the symmetries of the subgroup associated with the 2-dimensional (2D) Fe square sublattice, and thus on the low-energy features of the system, as for instance, the superconducting gap structure. Indeed, the standard  $C_{4v}$  group of the 2D square lattice, generated by the elementary  $\sigma_d$  and  $C_4$  point-group operations, does not fulfill all symmetries of the  $P4/nmm$  space-group, whereas the group generated by  $\sigma_d$  and  $S_4$  does. Moreover, proper ( $C_4$ ) and improper ( $S_4$ ) rotations differ from the physical point of view, because a Hamiltonian or a pairing function fulfilling the point-group operations generated by  $S_4$  and  $\sigma_d$  will transform in a very different way with respect to those based on the standard  $C_{4v}$  group, as it will be shown in the following.

From ab-initio electronic structure DFT and DMFT calculations of IBS,<sup>17–19</sup> it is well established that the bands crossing the Fermi level have a strong d-orbital character. Indeed,

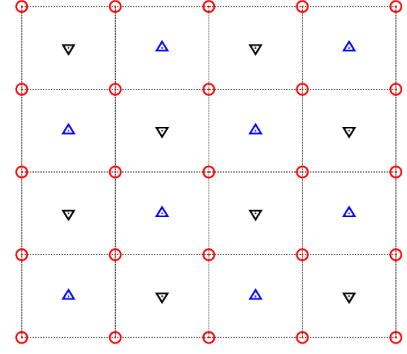


FIG. 1: Two dimensional square lattice representing the geometry of iron pnictides/chalcogenides planes in the tetragonal low temperature phase. The iron sites (red circles) form a perfect square lattice. The Se (As) atoms in e.g. FeSe (BaAs<sub>2</sub> Fe<sub>2</sub>) are below (lower triangles) or above (upper triangles) the iron layer. It is evident that a symmetry operation like rotation of 90 degrees around an iron atom, interchanges lower triangles with upper ones. Therefore a further reflection  $\sigma_h$  in the iron plane has to be combined with the 90 degree rotation to define a correct symmetry of the Hamiltonian. In a low energy model where Se and As atomic centers do not appear, their effect is to define a non trivial spatial symmetry in the iron square lattice where orbital and spatial degrees of freedom are strongly coupled in an unusual way. As noted in Ref. 49, also translation symmetry is not defined, but the composition of translation and reflection  $\sigma_h$  is again a well defined symmetry of the model. Then, the fictitious broken translation symmetry of the low energy model can be easily gauged out (see text and Ref. 22).

the minimal tight-binding Hamiltonian which reproduces successfully the Fermi surface contains all the five atomic (or Wannier) d-orbitals centered on the Fe sites,<sup>20</sup> namely  $|d_{xz}\rangle$ ,  $|d_{yz}\rangle$ ,  $|d_{xy}\rangle$ ,  $|d_{x^2-y^2}\rangle$ , and  $|d_{3z^2-r^2}\rangle$ , expressed with the crystal axes oriented according to the Fe square lattice directions. A given atomic orbital  $d_{\mathbf{R},\nu,\sigma}(\mathbf{r})$  defining the 2D multiorbital model can be represented by  $\langle \mathbf{r} | d_{\mathbf{R},\nu,\sigma} \rangle = \langle \mathbf{r} | c_{\mathbf{R},\nu,\sigma}^\dagger | 0 \rangle$ , where  $\mathbf{r}$  lives in the 3D space,  $\mathbf{R}$  is the center of the atomic orbital on the square lattice,  $\nu$  is the orbital symmetry, and  $\sigma = \pm \frac{1}{2}$  is the electron spin. A spatial point-group operation  $\eta$  acts on the orbital creation operator by changing its position  $\mathbf{R} \rightarrow R_\eta \mathbf{R}$ , its phase  $s = 1 \rightarrow s'(\eta, \nu) = \pm 1$  and its orbital label  $\nu \rightarrow \nu'(\eta, \nu)$  according to the general rule:

$$R_\eta c_{\mathbf{R},\nu,\sigma}^\dagger R_\eta^\dagger = s(\eta, \nu) c_{R_\eta \mathbf{R},\nu'(\eta,\nu),\sigma}^\dagger. \quad (1)$$

For  $\eta = \{\sigma_d, S_4, C_4\}$  and  $\nu$  given, the corresponding  $s'$  and  $\nu'$  are reported in Tab. I. The transformation rules are different, whether the group is generated by  $S_4$  or  $C_4$ .

As it is readily seen in Fig. (1), also the elementary translation symmetry bringing one iron atom to a nearest neighbor one, is not defined on the plane, because, under this transformation, the upper triangles are interchanged with the lower ones. Again the combination of the conventional translation  $T_x$  ( $T_y$ ) symmetry with the reflection  $\sigma_h$  is a well defined symmetry of the crystal  $\tilde{T}_x = \sigma_h T_x$  ( $\tilde{T}_y = \sigma_h T_y$ ), isomorphic to the conventional translation group of the square lattice. In a

$\nu$	$\eta = \sigma_d$	$\eta = S_4$	$\eta = C_4$
$d_{xz}$	$+d_{yz}$	$-d_{yz}$	$+d_{yz}$
$d_{yz}$	$+d_{xz}$	$+d_{xz}$	$-d_{xz}$
$d_{xy}$	$+d_{xy}$	$-d_{xy}$	$-d_{xy}$
$d_{x^2-y^2}$	$-d_{x^2-y^2}$	$-d_{x^2-y^2}$	$-d_{x^2-y^2}$
$d_{3z^2-r^2}$	$+d_{3z^2-r^2}$	$+d_{3z^2-r^2}$	$+d_{3z^2-r^2}$

TABLE I: Action of the symmetry operations  $\eta = \{\sigma_d, S_4, C_4\}$  on the five iron atomic d-orbitals. The entries represent the pair  $s' = \pm$  and  $\nu' = d_{xz}, d_{yz}, d_{xy}, d_{x^2-y^2}, d_{3z^2-r^2}$  as a function of the orbital index  $\nu$  (first column) and the symmetry operation  $\eta$  considered. Note the different  $s'$  between proper  $C_4$  and improper  $S_4$  rotations in the first two orbitals (odd with respect to  $\sigma_h$ ).

low energy model with a given number of orbitals  $\tilde{T}_x (\tilde{T}_y)$  behaves like the conventional translation group, only if we take into account a non-translation invariant sign in the definition of the localized basis, namely:

$$c_{\mathbf{R},\nu,\sigma}^\dagger \rightarrow (-1)^{x+y} c_{\mathbf{R},\nu,\sigma}^\dagger \quad (2)$$

for the orbitals  $\nu = \{d_{xz}, d_{yz}\}$  that are odd with respect to the symmetry operator  $\sigma_h$ . Here  $\mathbf{R} = (xa, ya)$ , where  $a$  is the lattice space of the square lattice. Unless otherwise specified, here and thereafter we use the translation invariant gauge defined in Eq. 2.

With these conventions, let us take into account the 2D tight-binding Hamiltonian  $H_0$  which defines the low-energy model for the IBS. Translation invariance means that all the coupling can be written in Fourier space:

$$\hat{H}_0 = \sum_{\mathbf{k},\nu,\mu,\sigma} t(\mathbf{k})_{\nu,\mu} c_{\mathbf{k},\nu,\sigma}^\dagger c_{\mathbf{k},\mu,\sigma}, \quad (3)$$

where the vectors  $\{\mathbf{k}\}$  belong to the unfolded Brillouin zone of the 2D lattice with one iron per unit cell,  $c_{\mathbf{k},\nu,\sigma}$  ( $c_{\mathbf{k},\nu,\sigma}^\dagger$ ) is the Fourier transform of  $c_{\mathbf{R},\nu,\sigma}$  ( $c_{\mathbf{R},\nu,\sigma}^\dagger$ ), the  $\mu, \nu$  indexes run over the d-orbital labels, the hoppings fulfill the hermitian condition  $t(\mathbf{k})_{\mu,\nu}^* = t(\mathbf{k})_{\nu,\mu}$ , and  $t(-\mathbf{k})_{\nu,\mu} = t(\mathbf{k})_{\nu,\mu}^*$  holds for reality. Without using the phase factor  $(-1)^{x+y}$  for the odd  $\sigma_h$  orbitals, the hopping between even and odd orbitals would have acquired an alternating sign, breaking the translation symmetry, as correctly pointed out in Ref. 49. After the simple gauge transformation given in Eq.(2) this fictitious broken symmetry is easily removed, and the low energy model becomes translational invariant, with a corresponding unfolded BZ.

In our approach we want to point out that a low energy two-dimensional model, like the free-band model in Eq.(3), has to be not only translation invariant but has to satisfy also all point symmetry transformations generated by  $\sigma_d$  and  $S_4$ , the compatible subgroup of the full  $P4/nmm$  space-group. The latter point group is isomorphic to the standard  $C_{4v}$  group of the square lattice provided, in this group, we identify the  $\pi/2$  rotation with the corresponding improper one.

If we apply the transformation rules in Eq. 1 to  $\hat{H}_0$ , and require its invariance, we obtain a set of relations for the hop-

ping matrix:

$$t(R_\eta \mathbf{k})_{\nu,\mu} = s(\eta, \nu) s(\eta, \mu) t(\mathbf{k})_{\nu'(\eta,\nu), \mu'(\eta,\mu)}, \quad (4)$$

for the eight possible independent point-group operations, defined by  $\eta = \sigma_d, S_4$ , and all their products. These transformations have already been derived in Refs. 21 and 22 or implicitly assumed in Refs. 48 and 7. However, their implications for the pairing properties have so far been overlooked.

The pairing operator  $\hat{F}$  is assumed to be translationally invariant (on the square lattice with one iron atom for unit cell and with the sign convention given in Eq. 2 for the odd reflection orbitals), so that it is convenient to write it in  $\mathbf{k}$ -space as

$$\hat{F} = \sum_{\mathbf{k},\nu,\mu} f(\mathbf{k})_{\nu,\mu} c_{\mathbf{k},\nu,\uparrow}^\dagger c_{-\mathbf{k},\mu,\downarrow}^\dagger. \quad (5)$$

Singlet pairing, and no broken time-reversal symmetry imply that  $f(\mathbf{k})_{\nu,\mu} = f(-\mathbf{k})_{\mu,\nu}$ , and  $f(\mathbf{k})_{\nu,\mu} = f(-\mathbf{k})_{\nu,\mu}^*$ , respectively. In the following, we derive the spatial-orbital properties of the pairing function  $F(\mathbf{r}, \mathbf{r}') = \langle \mathbf{r}, \mathbf{r}' | \hat{F} | 0 \rangle$ , by assuming that it belongs to the  $A_{1g}$  irreducible representation of the point-group generated by  $\sigma_d$  and  $S_4$ . This assumption will be verified later by ab-initio QMC calculations with a fully optimized Jastrow projected BCS wave function. “Improper s-wave” is the name we assign to the symmetry of the resulting  $\hat{F}$ , to distinguish it from the standard or “proper” one, i.e. the  $A_{1g}$  irreducible representation of the isomorphic point-group where the  $S_4$  class has been replaced by  $C_4$ .

Based on the general rules in Eq. 1 and the entries of Tab. I, we can derive the symmetry constraints for the improper s-wave. As the characters of the  $A_{1g}$  representation are - by definition - identically one for all classes within the point-group, the symmetry transformations of  $f(\mathbf{k})_{\nu,\mu}$  read as

$$f(R_\eta \mathbf{k})_{\nu,\mu} = s(\eta, \nu) s(\eta, \mu) f(\mathbf{k})_{\nu'(\eta,\nu), \mu'(\eta,\mu)}, \quad (6)$$

for  $\eta = \sigma_d, S_4$ , and all their independent products.

The above constraints reduce the variational freedom for the signs of  $F(\mathbf{r}, \mathbf{r}')$ . Accidental nodes must not break the *general* symmetries in Eq. 6. For the improper s-wave, we demonstrate that  $F$  has a peculiar, symmetry selected, sign structure. To show this, let us divide the iron d-orbitals into two groups, namely the “even” ( $e$ ) and “odd” ( $o$ ) ones, according to their parity under  $\sigma_h$ . The  $|d_{xz}\rangle$  and  $|d_{yz}\rangle$  orbitals are odd, while  $|d_{xy}\rangle$ ,  $|d_{x^2-y^2}\rangle$ , and  $|d_{3z^2-r^2}\rangle$  are even. Thus,  $F$  can be expanded as

$$F = F_{ee} + F_{eo} + F_{oe} + F_{oo}, \quad (7)$$

with its components defined as follows:

$$\begin{aligned} F_{ee}(\mathbf{r}, \mathbf{r}') &= \sum_{\mathbf{k}, \{\nu,\mu\} \in \text{even}} f(\mathbf{k})_{\nu,\mu} d_{\mathbf{k},\nu,\uparrow}(\mathbf{r}) d_{-\mathbf{k},\mu,\downarrow}(\mathbf{r}'), \\ F_{eo}(\mathbf{r}, \mathbf{r}') &= \sum_{\substack{\mathbf{k}, \{\nu\} \in \text{even} \\ \{\mu\} \in \text{odd}}} f(\mathbf{k})_{\nu,\mu} d_{\mathbf{k},\nu,\uparrow}(\mathbf{r}) d_{-\mathbf{k},\mu,\downarrow}(\mathbf{r}'), \\ F_{oe}(\mathbf{r}, \mathbf{r}') &= \sum_{\substack{\mathbf{k}, \{\nu\} \in \text{odd} \\ \{\mu\} \in \text{even}}} f(\mathbf{k})_{\nu,\mu} d_{\mathbf{k},\nu,\uparrow}(\mathbf{r}) d_{-\mathbf{k},\mu,\downarrow}(\mathbf{r}'), \\ F_{oo}(\mathbf{r}, \mathbf{r}') &= \sum_{\mathbf{k}, \{\nu,\mu\} \in \text{odd}} f(\mathbf{k})_{\nu,\mu} d_{\mathbf{k},\nu,\uparrow}(\mathbf{r}) d_{-\mathbf{k},\mu,\downarrow}(\mathbf{r}'). \end{aligned} \quad (8)$$

The above pairing functions are periodic in both  $\mathbf{r}$  and  $\mathbf{r}'$ , with periodicity set by the Bravais lattice vectors. In the following analysis, without loss of generality, we are going to pin  $\mathbf{r}$  around an iron site<sup>23</sup>, while we define  $F(k_x, k_y)$  as the 2D Fourier transform of  $F$  with respect to the planar  $(x, y)$  components of  $\mathbf{r}' - \mathbf{r}$ . According to the transformation rules in Eq. 6 and in Tab. I, we obtain that  $F_{ee}$  and  $F_{oo}$  have an s-wave planar symmetry, e.g.  $F_{ee}(k_x, k_y) = F_{ee}(-k_x, k_y) = F_{ee}(k_x, -k_y) = F_{ee}(k_y, k_x)$ , whereas  $F_{eo}$  and  $F_{oe}$ , which couple unlike-parity components, have planar  $d_{xy}$  symmetry, e.g.  $F_{eo}(k_x, k_y) = -F_{eo}(-k_x, k_y) = -F_{eo}(k_x, -k_y) = F_{eo}(k_y, k_x)$ . We note here that in a standard s-wave superconductor obeying the  $C_{4v}$  point-group transformations, also the  $F_{eo}$  and  $F_{oe}$  components are s-wave. Thus, our improper s-wave pairing function has to have different signs just from symmetry considerations. We note also that a two-band model containing only odd orbitals<sup>48</sup>, cannot account for the anomalous  $d_{xy}$  symmetry of the pairing function.

### III. AB-INITIO QUANTUM MONTE CARLO CALCULATION OF THE PAIRING FUNCTION OF $FeSe$

Our predictions presented in Sec. II and derived from symmetry arguments have been verified against accurate ab-initio QMC calculations based on the energy minimization of a Jastrow projected antisymmetrized geminal product (JAGP) wavefunction, performed for the  $FeSe$  on a  $4 \times 4 \times 1$  iron lattice, subject to periodic boundary conditions. The geminal or pairing function describes the spatial correlations in the singlet electron pairs, giving rise eventually to a superconducting state, if the pairing remains stable in the thermodynamic limit. We used the experimental  $FeSe$  geometry, determined at ambient pressure (0 GPa) and temperature<sup>24</sup> and under a hydrostatic pressure of 4 GPa at low-temperature.<sup>25</sup> Fe and Se atoms have been replaced by pseudoatoms, containing only 16 and 6 valence electrons, respectively.

#### A. Variational Jastrow projected AGP wave function

In this work, we used variational quantum Monte Carlo (QMC) methods to find the best many-body wave function  $\Psi$  which minimizes the variational energy

$$E = \langle \Psi | H | \Psi \rangle / \langle \Psi | \Psi \rangle, \quad (9)$$

where  $H$  is the electron first principles Hamiltonian in Hartree units

$$H = -\frac{1}{2} \sum_{i=1}^N \nabla_i^2 + \sum_{i,j=1}^N \frac{1}{|\mathbf{r}_i - \mathbf{r}_j|} - \sum_{i=1}^{N_{\text{nuclei}}} \sum_{j=1}^N v_i(\mathbf{R}_i - \mathbf{r}_j), \quad (10)$$

with  $N$  the number of electrons in the supercell,  $N_{\text{nuclei}}$  the number of nuclei, and  $\mathbf{R}_i$  the position of the  $i$ -th nucleus, fixed at the experimental geometry. In the Hamiltonian, the core electrons have been replaced by the pseudopotentials

$v_i$ . For iron, we used the energy-consistent scalar-relativistic Hartree-Fock pseudopotentials generated in Ref. 26, while for selenium, we used the smooth scalar-relativistic Hartree-Fock pseudopotentials published in Ref. 27. The system is unpolarized with  $N^\uparrow = N^\downarrow = N/2$ , and the supercell with  $N$  electrons is subject to periodic boundary conditions to reproduce the periodicity of the crystal, with standard Ewald summations of the long range Coulomb potential by including also the constant nucleus-nucleus interaction.

The wave function  $\Psi$  is written in the Jastrow projected AGP form

$$\Psi_{\text{JAGP}}(\mathbf{R}_{\text{el}}) = \exp[-J(\mathbf{R}_{\text{el}})] \det[\phi(\mathbf{r}_i^\uparrow, \mathbf{r}_j^\downarrow)], \quad (11)$$

where  $1 \leq i, j \leq N/2$ , and  $\mathbf{R}_{\text{el}} = \{\mathbf{r}_1^\uparrow, \dots, \mathbf{r}_{N/2}^\uparrow, \mathbf{r}_1^\downarrow, \dots, \mathbf{r}_{N/2}^\downarrow\}$  the many-body electron configuration. The variational form above has been widely used to study strongly correlated Hamiltonians on the lattice<sup>28-30</sup>, and then generalized to a large variety of ab-initio systems, ranging from molecules<sup>31-33</sup> to solids<sup>39,40</sup>. In all systems studied so far, it has been proven to be accurate and capable to describe strong charge localization, polarization effects and weak dispersive forces. The functional form in Eq. 11 is very flexible. The Jastrow factor  $J$  reads as

$$J(\mathbf{r}_1, \dots, \mathbf{r}_N) = \sum_{i=1}^{N_{\text{nuclei}}} \sum_{j=1}^N g_i^{\text{1-body}}(\mathbf{R}_i - \mathbf{r}_j) + \sum_{\substack{i,j=1 \\ i < j}}^N g(\mathbf{r}_i, \mathbf{r}_j), \quad (12)$$

where  $g_i^{\text{1-body}}$  is the electron-nucleus term, while  $g$  includes electron-electron correlations. We used a spin-independent parametrization for  $J$ , therefore the spin indexes are dropped out from Eq. 12. The one-body part is developed on Gaussian orbitals  $\chi_l^i$  (with  $l$  basis set index, and  $i$  nuclear index), and it depends on the  $i$ -th nucleus as follows

$$g_i^{\text{1-body}}(\mathbf{R}_i - \mathbf{r}) = \sum_l G_l^i \chi_l^i(\mathbf{R}_i - \mathbf{r}), \quad (13)$$

where the Gaussian basis set is built of  $2s2p/[1s1p]$  contracted  $\chi_l^i$  orbitals for selenium, while we used a  $2s2p2d/[1s1p1d]$  contracted Gaussian basis set for iron. Both  $G_l^i$ , the Gaussian exponents, and the linear coefficients of the contractions are variational parameters to be optimized. Note that there are no electron-nucleus cusps, as the pseudopotentials in Refs. 26 and 27 are finite at the origin. The electron-electron part  $g$  of the Jastrow factor is defined as

$$g(\mathbf{r}, \mathbf{r}') = u(|\mathbf{r} - \mathbf{r}'|) + \sum_{ijlm} H_{lm}^{ij} \chi_l^i(\mathbf{R}_i - \mathbf{r}) \chi_m^j(\mathbf{R}_j - \mathbf{r}'), \quad (14)$$

where the homogeneous part  $u(r) = 0.5r/(1 + \alpha r)$  fulfills the electron-electron cusp conditions for unlike-spin particles, and the Gaussian basis sets  $\chi_l^i$  are the same as the ones in the one-body part.  $\alpha$  and the symmetric matrix  $H_{lm}^{ij}$  are variational parameters. The basis set parameters (Gaussian exponents and the linear coefficients) are optimized together with the one-body part.

The pairing function  $\phi$  in Eq. 11 reads as

$$\phi(\mathbf{r}, \mathbf{r}') = \sum_{i=1}^M \lambda_i \psi_i^{MO}(\mathbf{r}) \psi_i^{MO}(\mathbf{r}'), \quad (15)$$

where the sum is over  $M(\geq N/2)$  molecular orbitals  $\psi_i^{MO}(\mathbf{r})$ , where each one can be occupied by opposite spin electrons. The orbitals  $\psi_i^{MO}(\mathbf{r})$  are expanded in a Gaussian single-particle basis set  $\{\chi_j^{\text{det}}\}$ , centered on the atomic nuclei as in the Jastrow case, i.e.

$$\psi_i^{MO}(\mathbf{r}) = \sum_j K_{ij} \chi_j^{\text{det}}(\mathbf{r}), \quad (16)$$

where the sum in the above equation runs over both the basis set and nuclear center indexes (for simplicity of notations we omit here the explicit dependence on the atomic positions). The  $\{\chi_i^{\text{det}}\}$  basis set is uncontracted with size of  $9s8p7d6f$  for Fe and  $6s5p4d3f$  for Se.  $\lambda_i$ ,  $K_{ij}$ , and the exponents of the uncontracted Gaussian basis set  $\{\chi_j^{\text{det}}\}$  are variational parameters. If  $M = N/2$ , the expansion in Eq. 15 is equivalent to a single Slater determinant, when the antisymmetrization of  $\phi$  is performed. On the other hand, if  $M > N/2$ , correlation is introduced through the pairing function, and one can describe the effective attraction between opposite spin electrons by a reduction of the total variational energy. If this energy gain survives in the thermodynamic limit, it implies that the BCS condensate formed by the electron singlets is stable, and the symmetry of the pairing function is the one of the superconducting gap.

In order to treat the periodic system in a finite supercell, both the Jastrow Gaussian basis set  $\{\chi_l^i\}$  and the one  $\{\chi_j^{\text{det}}\}$  of the pairing function  $\phi$  are made of periodic Gaussian functions, as described in Ref. 39.

## B. Numerical methods

To generate the initial molecular orbitals, we performed preliminary density functional theory (DFT) calculations in the local density approximation, within the same basis described in the previous subsection. The starting Gaussian exponents of the  $\{\chi_j^{\text{det}}\}$  basis are even-tempered, as they are defined as  $Z_i = \alpha \beta^i$  for  $i = 0, \dots, n-1$  with  $\alpha = Z_{\min}$  and  $\alpha \beta^n = Z_{\max}$ . The number of Gaussians  $n$ ,  $Z_{\min}$  and  $Z_{\max}$  are optimized independently for each angular momentum shell in order to minimize the total DFT energy. The number of shells, and the number of Gaussians per shell are chosen to give a convergence of  $\approx 10$  mHartree per iron atom in the DFT energy.<sup>41</sup>

The MO generated by DFT are then used to build the  $\Psi_{\text{JAGP}}$  wave function. At the beginning, the pairing function is such that  $\lambda_i = 1$  for  $i \leq N/2$  and  $\lambda_i = 0$  for  $i > N/2$ , i.e. we start from a Jastrow-Slater wave function, with the Slater part exactly given by the DFT orbitals and with no Jastrow factor ( $H_{lm}^{ij} = G_l^i = 0$ ) apart from an initial guess of the variational constant  $\alpha \approx 1$  in its homogeneous part  $u$ . The many-body

wave function is optimized in the QMC framework by minimizing the variational energy in Eq. 9, by using the stochastic reconfiguration (SR) method (based on the first-order derivatives of the energy with respect to the variational parameters) combined with second-order contributions coming from the Hessian matrix (“linear method”). Indeed, the SR method described in Ref. 31 has been improved by using a statistically more accurate evaluation of the Hessian matrix elements in the so called “linear basis” as described in Ref. 42. Before the full optimization of all the variational parameters in our JAGP wave function, we adopt the following intermediate steps:

- i) first the Jastrow linear coefficients  $G_l^i$  and  $H_{lm}^{ij}$ , together with the parameter  $\alpha$  of the homogeneous pairwise Jastrow factor, are optimized;
- ii) then, also the linear coefficients of the Jastrow basis contractions  $\{\chi_l^i\}$  are optimized;
- iii) not only the contraction coefficients but also the Jastrow Gaussian exponents are relaxed, together with all previous parameters, by means of the linear minimization method;
- iv) finally, all variational parameters (in both the Jastrow and the Slater determinant) are optimized. In this last step the molecular orbitals evolve according to the algorithm described in Ref.43, that allows one to exploit the derivatives with respect to their atomic (uncontracted) components without changing the rank of the full pairing matrix. In the last step, in order to decrease the number of variational parameters involved in the uncontracted basis for the AGP, we perform the minimization by using only one contracted orbital for each angular momentum. This allows us to represent in the most efficient way the correction to the DFT orbitals. With this strategy we achieve a dramatic reduction of the number of parameters and a systematic improvement of the variational energy, which substantially decreases with respect to step (iii).

Once the best Jastrow correlated single determinant wave function is obtained, we let the wave function develop a singlet pairing correlation, by expanding it beyond the single Slater determinant. We add in Eq. 15 the first  $M - N/2$  additional DFT MO orbitals above the Fermi level, with their corresponding  $\lambda_i$  (with  $i$  s.t.  $N/2 < i \leq M$ ) taken from an educated guess based on a BCS-like estimate of the pairing amplitude, and later fully optimized. The optimal  $M$  is chosen to match the criterion discussed in Ref. 43, namely it is the sum of the majority spin orbitals in the atomic limit ( $M = \sum_{i=1}^{N_{\text{nuclei}}} n_i^{\uparrow}$ , where we take the convention that  $n_i^{\uparrow} \geq n_i^{\downarrow} \forall i$  in the dissociation limit). The final global optimization is performed with the same method used before in (iv), with all parameters free to move, and the convergence of the  $\Psi_{\text{JAGP}}$  is reached if the variation of  $\lambda_i$  with  $i > N/2$  is within the statistical noise. Note that the hierarchy followed in the wave function optimization is related to the energy scale of its various components, the smallest and the last one being the energy gain (also called “condensation energy”) due to the

paired state with respect to the Fermi liquid reference, namely  $\lambda_i = 0$  for  $i > N/2$ .

The final wave function yields invaluable information about the correlated ground state, like the symmetry of the superconducting gap, in the case that a paired state is stabilized by the variational approach. This method is unbiased, as we do not provide any constraint in the energy minimization, except for the symmetries imposed by the translational invariance of the lattice structure, which reduce the total number of independent variational parameters. In a large variety of systems studied by this wave function, we reached the chemical accuracy (in the energy differences), without resorting to further projective methods like diffusion Monte Carlo. We would like also to highlight the fact that this variational method is sign problem free.

For the largest system computed, the FeSe  $4 \times 4 \times 1$  lattice (16 Fe + 16 Se) with 352 electrons, a full QMC energy minimization has been performed to optimize a total amount of about 10000 independent variational parameters.

### C. Results

The full many-body wave function is written in a compact form as in Eq. 11. In all the calculations quantum effects on nuclei are neglected, within the Born-Oppenheimer approximation. Hence superconductivity is assumed to be non conventional, namely not coming from electron-phonon coupling.

$\phi(\mathbf{r}, \mathbf{r}')$ , defining the wave function in Eq. (11), is an extension of  $F(\mathbf{r}, \mathbf{r}')$  in Eq. 7, as it is expanded over the full atomic basis set used to represent the MO's. The resulting  $\phi$ , restricted to its correlated part  $\phi^{corr}$  (obtained by summing the MOs in Eq. 15 over  $i$  with  $N/2 < i \leq M$ ), is plotted in Figs. 2 and 3 for 0 and 4 GPa, respectively.  $\phi^{corr}$  has been projected over its 4 possible components  $\phi_{ee}^{corr}$  (Figs. 2(a) and 3(a)),  $\phi_{oo}^{corr}$ ,  $\phi_{eo}^{corr}$ , and  $\phi_{oe}^{corr}$  (Figs. 2(b) and 3(b)), based on the parity with respect to  $\sigma_h$ <sup>44</sup>.

The final picture is consistent with the improper s-wave pairing function predicted by the 2D point-group symmetries and under the assumption of a 3D  $A_{1g}$  irreducible representation. Our QMC solution is  $A_{1g}$  as a consequence of an unbiased energy minimization, and it has not been imposed a priori in the optimization. Thanks to the improper  $S_4$  generated point-group, the pairing function  $\phi$  shows two planar symmetry channels, s-wave for the  $\phi_{ee}^{corr}$  and  $\phi_{oo}^{corr}$ ,  $d_{xy}$ -wave for the  $\phi_{eo}^{corr}$  and  $\phi_{oe}^{corr}$  components. We emphasize that  $\phi$  does not possess a well defined symmetry under a proper rotation by  $\pi/2$ , just because such a rotation is not a symmetry of the crystal. Moreover, Fig. 3 shows that this picture holds even when the tetragonal point-group symmetry is slightly broken, and lowered to the orthorhombic point-group, as in the case of applied pressure and/or low temperature.

To further check the reliability of  $\Psi_{JAGP}$  to describe the superconducting features of FeSe, we estimated (via correlated sampling) the condensation energy  $\epsilon_{cond}$ , defined as the difference (per iron atom) between the expectation value of  $H$  computed with the fully paired  $\Psi_{JAGP}$  and the one with the Jastrow projected single determinant, obtained by summing

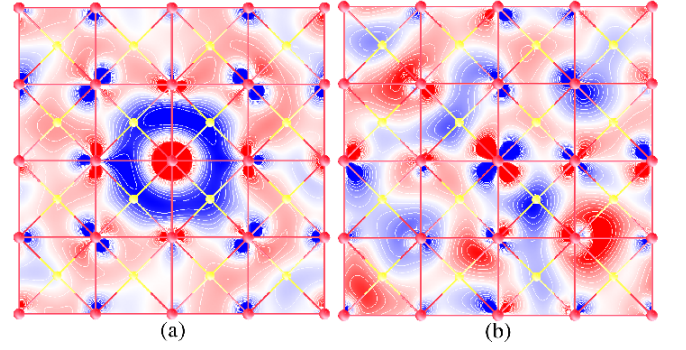


FIG. 2: Even-even (panel a), and odd-even (panel b) components of the pairing function  $\phi^{corr}$  of the FeSe high- $T_c$  superconductor at 0 GPa obtained by QMC, by optimizing the energy of the variational wavefunction without assuming any point symmetry. The contour plots show  $\phi^{corr}(\mathbf{R}_{center}, \mathbf{r})$  with  $\mathbf{R}_{center}$  set to be the iron lattice site at the center of the supercell, while  $\mathbf{r}$  spans the plane defined by the  $4 \times 4$  lattice. Red (yellow) balls are iron (selenium) sites. Arbitrary units blue (red) intensity indicates negative (positive) regions with corresponding magnitude.

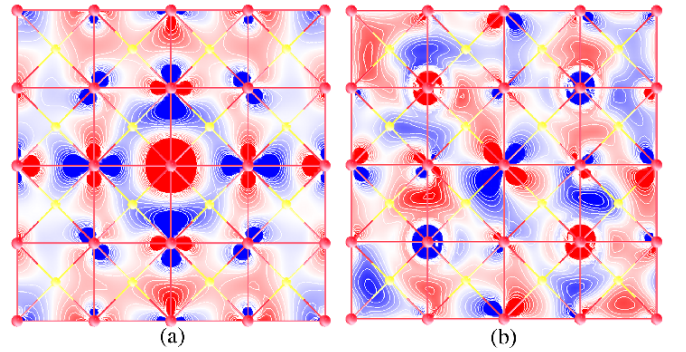


FIG. 3: The same as in Fig. 2 but for a structure corresponding to a pressure of 4 GPa.

the MOs with  $i \leq N/2$  in Eq. 15. Those quantities are much more sensitive to finite size errors than the pairing symmetry, set by the short-range behavior of  $\phi$ , which is converged in the  $4 \times 4$  supercell. The  $\epsilon_{cond}$  is shown in Fig. 4, together with the experimental critical temperature  $T_c$ . It turns out that  $\epsilon_{cond} \approx 6k_B T_c$ , which is a remarkable result given the tiny energy scale (of the order of 1 meV) involved in the gap opening.<sup>45</sup> Moreover, it follows quite well the behavior of the experimental  $T_c$ , which increases with pressure, in the pressure range considered here<sup>45</sup>. Therefore, if we assume that the condensation energy should be related to the critical temperature, as it is a common feature of high- $T_c$  superconductors, our pairing function describes reasonably well the experiments. Remarkably, we are close to make quantitative predictions on unconventional high temperature superconductors by means of a fully ab-initio method.



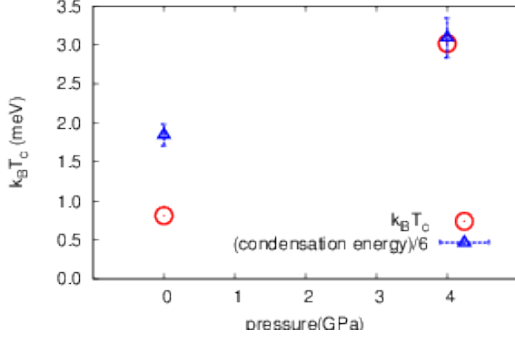


FIG. 4: Condensation energy in the  $4 \times 4$  system (in Hartree), and pairing gap  $\Delta_{BCS}$  (in meV) at 0 and 4 GPa, obtained from our QMC calculations, compared to the experimental superconducting temperature  $T_c$  in meV.

#### IV. BCS MODELING OF THE QMC PAIRING FUNCTION

The determinantal part of our JAGP variational wave function, for technical reasons, has not a simple interpretation in terms of a mean-field BCS Hamiltonian, as it is common practice in lattice model calculations of strongly correlated systems<sup>30,34</sup>. In this case, it is well known that very few short range parameters can describe very accurately the gap function  $\Delta(\mathbf{k})$  of a correlated superconductors. Moreover, whenever the variational description is accurate enough, very small supercells are necessary to describe non trivial physical effects and also phase transitions<sup>35</sup>. For the above reasons, it is therefore extremely important to describe our variational wave function in terms of a mean-field BCS picture, because it helps to reduce the finite size effects. Otherwise, a brute force variational approach based on the JAGP, would require high resolution in momentum space, and therefore too large supercells, to describe correctly the opening of the superconducting gap over the non trivial and rather involved hole and electron Fermi surfaces of pnictides. For example, we will show in the

following Subsections, that a short range parametrization of an improper s-wave gap function represents in a quantitative way our paired variational state. This is extremely useful to obtain a detailed information in  $\mathbf{k}$ -space, and finally provides a rather satisfactory description of the realistic material.

##### A. BCS model Hamiltonian and pairing function

We start with the five band model defined on the iron plane in real space:

$$H_{BCS} = \sum_{ij,\mu,\nu,\sigma} t(\mathbf{R}_i - \mathbf{R}_j)_{\mu,\nu} c_{\mathbf{R}_i,\mu,\sigma}^\dagger c_{\mathbf{R}_j,\nu,\sigma} + \sum_{ij,\mu,\nu} \Delta(\mathbf{R}_i - \mathbf{R}_j)_{\mu,\nu} c_{\mathbf{R}_i,\mu,\uparrow}^\dagger c_{\mathbf{R}_j,\nu,\downarrow}^\dagger + \text{h.c.} \quad (17)$$

We assume no broken time reversal symmetry and therefore all couplings are real, including the BCS ones, and singlet pairing. Thus both  $t$  and  $\Delta$  have to be considered symmetric real matrices.

Due to translation invariance the model is more easily written in  $\mathbf{k}$ -space:

$$H_{BCS} = \sum_{k,\mu,\nu,\sigma} t(\mathbf{k})_{\mu,\nu} c_{\mathbf{k},\mu,\sigma}^\dagger c_{\mathbf{k},\nu,\sigma} + \sum_{k,\mu,\nu} \Delta(\mathbf{k})_{\mu,\nu} c_{\mathbf{k},\mu,\uparrow}^\dagger c_{-\mathbf{k},\nu,\downarrow}^\dagger + \text{h.c.} \quad (18)$$

It is easy to show that, for each  $\mathbf{k}$ , both matrices  $t$  and  $\Delta$  may be complex, but they have to be hermitian. In  $\mathbf{k}$ -space the relations in Tab.(I) imply parity symmetry constraints on the  $t(\mathbf{k})$  matrix elements, as we have seen in Sec. II. The same constraints hold for the BCS pairing matrix  $\Delta(\mathbf{k})$ . In case of a "generalized"  $A_{1g}$  real pairing (dubbed here "improper s-wave") the symmetry relations are the following:

$$\begin{aligned}
\Delta_{\mu,\mu}(k_x, k_y) &= \Delta_{\mu,\mu}(\pm k_x, \pm k_y) = \Delta_{\mu,\mu}(k_y, k_x) & \text{for } \mu \neq xz, yz \\
\Delta_{\mu,\mu}(k_x, k_y) &= \Delta_{\mu,\mu}(\pm k_x, \pm k_y) & \text{for } \mu = xz, yz \\
\Delta_{xz,xz}(k_x, k_y) &= \Delta_{yz,yz}(k_y, k_x) \\
\Delta_{xz,yz}(k_x, k_y) &= -\Delta_{xz,yz}(-k_x, k_y) = -\Delta_{xz,yz}(k_x, -k_y) = \Delta_{yz,xz}(k_y, k_x) \\
\Delta_{xz,x^2-y^2}(k_x, k_y) &= \Delta_{xz,x^2-y^2}(-k_x, k_y) = -\Delta_{xz,x^2-y^2}(k_x, -k_y) \\
\Delta_{yz,x^2-y^2}(k_x, k_y) &= -\Delta_{yz,x^2-y^2}(-k_x, k_y) = \Delta_{yz,x^2-y^2}(k_x, -k_y) = -\Delta_{xz,x^2-y^2}(k_y, k_x) \\
\Delta_{xz,xy}(k_x, k_y) &= -\Delta_{xz,xy}(-k_x, k_y) = \Delta_{xz,xy}(k_x, -k_y) \\
\Delta_{yz,xy}(k_x, k_y) &= \Delta_{yz,xy}(-k_x, k_y) = -\Delta_{yz,xy}(k_x, -k_y) = \Delta_{xz,xy}(k_y, k_x) \\
\Delta_{xz,z^2}(k_x, k_y) &= \Delta_{xz,z^2}(-k_x, k_y) = -\Delta_{xz,z^2}(k_x, -k_y) \\
\Delta_{yz,z^2}(k_x, k_y) &= -\Delta_{yz,z^2}(-k_x, k_y) = \Delta_{yz,z^2}(k_x, -k_y) = \Delta_{xz,z^2}(k_y, k_x) \\
\Delta_{x^2-y^2,xy}(k_x, k_y) &= -\Delta_{x^2-y^2,xy}(-k_x, k_y) = -\Delta_{x^2-y^2,xy}(k_x, -k_y) = -\Delta_{x^2-y^2,xy}(k_y, k_x) \\
\Delta_{x^2-y^2,z^2}(k_x, k_y) &= \Delta_{x^2-y^2,z^2}(-k_x, k_y) = \Delta_{x^2-y^2,z^2}(k_x, -k_y) = -\Delta_{x^2-y^2,z^2}(k_y, k_x) \\
\Delta_{xy,z^2}(k_x, k_y) &= -\Delta_{xy,z^2}(-k_x, k_y) = -\Delta_{xy,z^2}(k_x, -k_y) = \Delta_{xy,z^2}(k_y, k_x)
\end{aligned} \tag{19}$$

Notice that, by the no broken time reversal condition (real space couplings, i.e.  $t(\mathbf{k}) = t^*(-\mathbf{k})$ ,  $\Delta(\mathbf{k}) = \Delta^*(-\mathbf{k})$ ), the above functions are purely real or purely imaginary depending on the transformation under reflection, even ( $\Delta_{\mu,\nu}(\mathbf{k}) = +\Delta_{\mu,\nu}(-\mathbf{k})$ ) or odd ( $\Delta_{\mu,\nu}(\mathbf{k}) = -\Delta_{\mu,\nu}(-\mathbf{k})$ ), respectively.

A generic quasiparticle with spin up can be written as:

$$\psi_{\mathbf{k},\nu,\uparrow}^\dagger = \sum_{\mu} u_{\mu,\nu} c_{\mathbf{k},\mu,\uparrow}^\dagger + v_{\mu,\nu} c_{-\mathbf{k},\mu,\downarrow} \tag{20}$$

where  $u$  and  $v$  are arbitrary complex  $5 \times 5$  matrices, satisfying:

$$\begin{aligned}
u^\dagger u + v^\dagger v &= I \\
u^\dagger v - v^\dagger u &= 0
\end{aligned} \tag{21}$$

In order to compute these matrices it is enough to write the quasiparticle equation:

$$[H_{BCS}, \psi_{\mathbf{k},\nu,\uparrow}^\dagger] = E_\nu(\mathbf{k}) \psi_{\mathbf{k},\nu,\uparrow}^\dagger \tag{22}$$

which implies to solve a  $10 \times 10$  eigenvalue problem for each

$\mathbf{k}$ :

$$\begin{vmatrix} t(\mathbf{k}) & \Delta(\mathbf{k}) \\ \Delta(\mathbf{k}) & -t(\mathbf{k}) \end{vmatrix} \begin{vmatrix} u_\nu \\ v_\nu \end{vmatrix} = E_\nu(\mathbf{k}) \begin{vmatrix} u_\nu \\ v_\nu \end{vmatrix} \tag{23}$$

Notice that Eq. 23 has pairs of eigenvalues of opposite values as if  $(u, v)$  is an eigenvector with eigenvalue  $E(\mathbf{k})$ ,  $(v, -u)$  has eigenvalue  $-E(\mathbf{k})$ . Thus we have 5 positive and 5 negative eigenvalues for each  $\mathbf{k}$ . The pairing function  $f^{BCS}$  defines the ground state  $\Psi_{BCS}$  of the BCS Hamiltonian by:

$$|\Psi_{BCS}\rangle = \exp\left(\sum_{\mu,\nu} f^{BCS}(\mathbf{k})_{\mu,\nu} c_{\mathbf{k},\mu,\uparrow}^\dagger c_{-\mathbf{k},\nu,\downarrow}^\dagger\right) |0\rangle \tag{24}$$

The function  $f^{BCS}$  can be determined by requiring that the ground state is the vacuum of all the quasiparticles with positive eigenvalues:

$$\psi_{\mathbf{k},\nu,\uparrow} |\Psi_{BCS}\rangle = 0 \tag{25}$$

for all eigenvalues  $E_\nu(\mathbf{k}) > 0$ . By using that

$$\exp(-F^\dagger) \psi_{\mathbf{k},\nu,\uparrow} \exp(F^\dagger) = \sum_{\mu} \left\{ u_{\nu,\mu}^\dagger c_{\mathbf{k},\mu,\uparrow} + [(u^\dagger f^{BCS})_{\nu,\mu} + v_{\nu,\mu}^\dagger] c_{-\mathbf{k},\mu,\downarrow}^\dagger \right\}, \tag{26}$$

where  $F^\dagger = \sum_{\mu,\nu} f^{BCS}(\mathbf{k})_{\mu,\nu} c_{\mathbf{k},\mu,\uparrow}^\dagger c_{-\mathbf{k},\nu,\downarrow}^\dagger$ , we finally obtain that the matrix  $f^{BCS}$  is fully determined via the quasiparticle equation. By solving  $u^\dagger f^{BCS} + v^\dagger = 0$ , it reads:

$$f^{BCS}(\mathbf{k}) = -(u^\dagger)^{-1} v^\dagger, \tag{27}$$

namely, for each  $\mathbf{k}$ ,  $f^{BCS}$  is a generally full  $5 \times 5$  matrix. From Eq.(21) it also follows that  $f^{BCS}(\mathbf{k})$  is hermitian for each  $\mathbf{k}$  and can therefore be diagonalized with real eigenvalues. This property is the final consequence of the assumed no broken time reversal symmetry, otherwise  $f^{BCS}$  is only a symmetric matrix, generally complex.



## B. BCS fitting of the QMC pairing function

We use the BCS model of Eq. 17 as a way to interpolate on an ultra dense k-grid the realistic pairing  $f$  which enters the JAGP wave function, computed on a  $4 \times 4$  k-point mesh by the ab-initio variational QMC method as described in Sec. III. Within the BCS framework, we fit both the tight-binding model and the effective BCS coupling  $\Delta$  from ab-initio calculations. The tight-binding model in Eq. 18 is fitted based on the Wannier interpolation of the LDA-DFT band structure<sup>36</sup> calculated for the undistorted ambient pressure FeSe compound. The number of neighbors taken in the model is the same as the one used in Ref. 20 by Graser *et al.*. On the other hand, we assume a short-range BCS  $\Delta$ , by taking only the nearest-neighbors couplings, assumption that is normally verified for strongly correlated superconductors. Those couplings are set to reproduce the real space image of the ab-initio QMC pairing function  $\phi^{corr}(\mathbf{r}, \mathbf{r}')$  plotted in Fig. 2. We define the real-space BCS pairing function as:

$$F^{BCS}(\mathbf{r}, \mathbf{r}') = \sum_{\mathbf{k}, \nu, \mu} f^{BCS}(\mathbf{k})_{\nu, \mu} d_{\mathbf{k}, \nu, \uparrow}^G(\mathbf{r}) d_{-\mathbf{k}, \mu, \downarrow}^G(\mathbf{r}'), \quad (28)$$

where  $f^{BCS}(\mathbf{k})_{\nu, \mu}$  is the solution of the BCS problem (18) on a given k-grid as in Eq. 27, and  $d_{\mathbf{k}, \nu, \uparrow}^G(\mathbf{r})$  are localized functions taken as Gaussian periodic orbitals with d-symmetry<sup>39</sup> and Gaussian exponent  $Z = 0.8$ . Moreover, according to Eq. (2), an overall sign  $(-1)^{x+y}$  is given to the localized Wannier orbitals, centered at  $\mathbf{R} = (ax, ay)$  and with odd reflection symmetry. This essentially implies that  $d_{\mathbf{k}, \nu, \uparrow}^G(\mathbf{r}) \rightarrow d_{\mathbf{k}+\mathbf{Q}, \nu, \uparrow}^G(\mathbf{r})$ , for such odd reflection orbitals, where  $\mathbf{Q} = (\pi, \pi)$ . In this way the anomalous part of the pairing function  $F_{eo} + F_{oe}$  that connects even and odd  $s_h$  orbitals, breaks the translation symmetry because couples  $\mathbf{k}$  and  $\mathbf{k} + \mathbf{Q}$  physical momenta. However, this broken translation symmetry, noticed in Refs. 49 and 22, can be completely gauged out in the low energy 2D model, and is not so crucial therefore (e.g. absolutely irrelevant for the spectrum), as the improper s-wave symmetry we are pointing out in this work.

We choose the non-zero couplings  $\Delta$  in Eq. 17 such that  $F^{BCS}(\mathbf{r}, \mathbf{r}')$  is as close as possible to the QMC  $\phi^{corr}(\mathbf{r}, \mathbf{r}')$  in the largest QMC supercell, by minimizing the distance in the  $L2$  functional space. This is obtained by maximizing the normalized scalar product  $F^{BCS} \cdot \phi^{corr} / \sqrt{\|F^{BCS}\| \|\phi^{corr}\|}$ , which in the Gaussian basis reads:

$$\frac{\text{Tr}[S f^{BCS} S \tilde{\phi}^{corr}]}{\sqrt{\text{Tr}[S f^{BCS} S f^{BCS}] \text{Tr}[S \tilde{\phi}^{corr} S \tilde{\phi}^{corr}]}} \quad (29)$$

where  $\tilde{\phi}^{corr}$  is the projection of  $\phi^{corr}$  on the single Gaussian basis set  $d_{\mathbf{R}, \nu}^G(\mathbf{r})$ , and  $S = S(\mathbf{R})_{\mu\nu} = \langle d_{\mathbf{0}, \mu}^G | d_{\mathbf{R}, \nu}^G \rangle$  is the overlap matrix between the basis set elements. The largest normalized scalar product found is about 50%, with best cou-

plings which turn out to be (in eV):

$$\begin{aligned} \Delta_{xz, xz}(\delta \mathbf{R}_x) &= \Delta_{yz, yz}(\delta \mathbf{R}_y) = -0.080 \\ \Delta_{xz, xz}(\delta \mathbf{R}_y) &= \Delta_{yz, yz}(\delta \mathbf{R}_x) = -0.051 \\ \Delta_{xy, xy}(\delta \mathbf{R}_x) &= \Delta_{xy, xy}(\delta \mathbf{R}_y) = 0.158 \\ \Delta_{z^2, z^2}(\delta \mathbf{R}_x) &= \Delta_{z^2, z^2}(\delta \mathbf{R}_y) = -0.0163 \\ \Delta_{x^2-y^2, z^2}(\delta \mathbf{R}_x) &= -\Delta_{x^2-y^2, z^2}(\delta \mathbf{R}_y) = 0.0035 \\ \Delta_{xz, xy}(\delta \mathbf{R}_x) &= \Delta_{yz, xy}(\delta \mathbf{R}_y) = -0.130, \end{aligned} \quad (30)$$

where  $\delta \mathbf{R}_x = (\delta, 0)$ ,  $\delta \mathbf{R}_y = (0, \delta)$ , with  $\delta$  the distance between two nearest-neighbors iron sites. The last one in Eq. 30 is the even-odd/odd-even coupling which triggers the planar d-wave component and leads to the improper s-wave symmetry of the global pairing.

It is interesting to note that the resulting pairing  $f(\mathbf{k})_{\mu, \nu}$  is purely real if it couples even-even and odd-odd orbitals, while it is purely imaginary when it couples even-odd and odd-even orbitals. This follows from the  $t(\mathbf{k})$  and  $\delta(\mathbf{k})$  components, which are either purely real or purely imaginary according to their transformation properties, as already highlighted in the previous Subsection.

In the literature, the k-resolved image of the coupling and its symmetry analysis provided so far, are usually done for the  $\tilde{f}(\mathbf{k})_{m, n}$  pairing function projected and rotated in the band space (here  $m$  and  $n$  refer to band indexes), i.e.  $\tilde{f}(\mathbf{k}) = U^\dagger(\mathbf{k}) f(\mathbf{k}) U(\mathbf{k})$ , with  $U$  the unitary matrix mapping the orbital into the band space. We stress that the band space is not the ideal basis to study the improper s-wave symmetry, as only the orbitals are eigenstates of the parity under reflection through the iron plane. The hybrid nature of the bands does not allow to separate the planar s- and d-wave components of the total pairing operator  $\hat{F}$  in Eq. 5. In the next section, we will analyze in detail the k-resolved components of  $F$  in the orbital basis and the superconductivity gap of the associated BCS model. Here, we provide the k-resolved image of  $\tilde{f}(\mathbf{k})_{m, n}$  in the band basis on the Fermi surface, in order to understand its sign properties, and compare it with the previous literature.

In Fig. 5 we plot  $\tilde{f}(\mathbf{k})_{m, n}$  with  $\mathbf{k}$ 's on the Fermi surface (in the unfolded Brillouin zone), which results from the BCS model interpolation on an ultra dense  $200 \times 200$  k-point grid. The Figure shows that the global symmetry is the  $A_{1g}$ . The only sign change in this picture occurs within the M electron pockets, already pointed out in previous works<sup>6,7</sup>. However, once the global symmetry is fixed, the  $\tilde{f}$  components can have in general a non trivial structure, which is material dependent, due to its multi-band nature. Here, we find that for the FeSe there are no other sign changes except for the ones in the M pocket. It is hard to say if this comes from the improper s-wave symmetry or the sign change is just "accidental". In the band representation, there is not a clear-cut signature of the improper s-wave components.

In the next section, we are going to analyze what are the symmetry implications of the improper-s symmetry, by studying the full pairing function  $F$  in the orbital space and its related BCS gap.

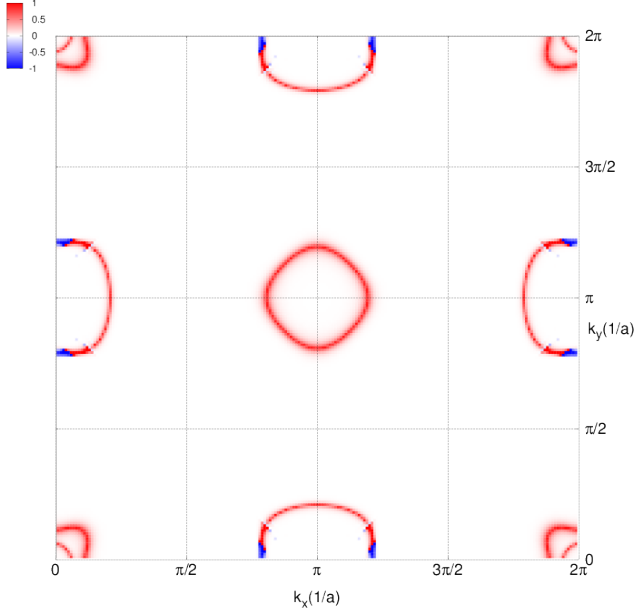


FIG. 5: Fermi surface projection of  $\sum_n \tilde{f}(\mathbf{k})_{n,n}$  plotted on the unfolded Brillouin zone (one Fe unit cell).

### C. k-resolved image of the BCS gap function and physical pairing

The BCS model derived in the previous Subsection allows not only to interpolate  $f(\mathbf{k})_{\mu,\nu}$  on a dense k-point grid, but also to evaluate the k-resolved BCS gap  $\Delta^{BCS}(\mathbf{k})$ , of paramount importance to make a connection with some angle-resolved experiments as for instance the specific heat measurements performed in Ref. 15 for the FeSe. That experiment indicates the presence of gap minima along the  $\Gamma$ -M (Fe-Fe) bond directions, and conversely the gap maxima along the Fe-Se-Fe directions, being the angular dependence fourfold.

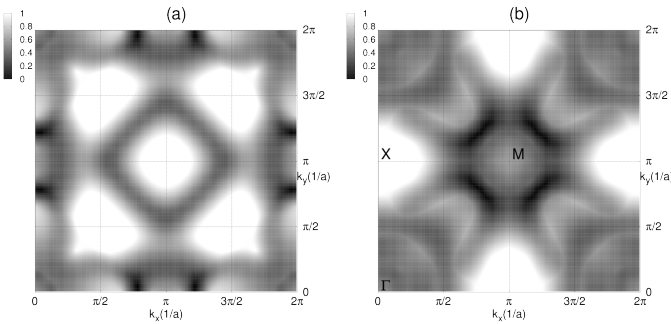


FIG. 6: BCS gap computed in eV on a  $200 \times 200$  k-point grid in the unfolded (panel (a)) and folded (panel (b)) Brillouin zone

Fig. 6 obtained on a  $200 \times 200$  k-point grid from the solution of the BCS model with parameters in Subsec. IV B shows that indeed minima are aligned in the  $\Gamma$ -M directions, while

maxima are clearly peaked along the X-M directions, in general agreement with the specific heat experiment.

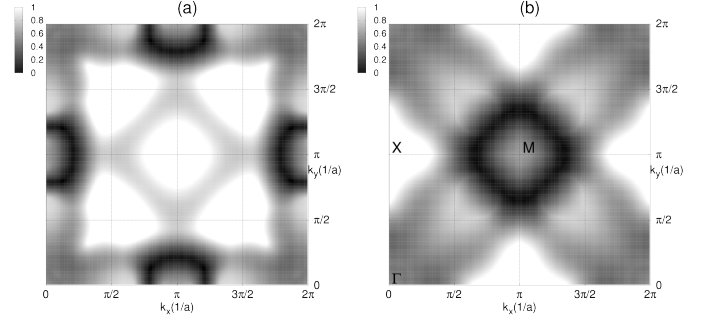


FIG. 7: BCS gap computed in eV on a  $200 \times 200$  k-points grid in the unfolded (panel (a)) and folded (panel (b)) Brillouin zone by setting  $\Delta_{xz,xy}$  and  $\Delta_{yz,xy}$  to zero.

To understand the role of the even-odd/odd-even couplings in setting the gap modulation, we explicitly set to zero  $\Delta_{xz,xy}$  and  $\Delta_{yz,xy}$  in Eq. 30, while keeping unchanged the other BCS parameters. The resulting BCS gap of this modified model is shown in Fig. 7. As one can see, the angular dependence of the BCS gap minima (black regions) of the latter model is much more isotropic. Thus, the  $\Delta_{xz,xy}$  and  $\Delta_{yz,xy}$  BCS parameters, which couple orbitals of different parity, play a key role to trigger the angular dependence of the BCS gap.

We turn now our attention to the Fourier analysis of the physical pairing function  $F(\mathbf{r}, \mathbf{r}') = \langle \mathbf{r}, \mathbf{r}' | \hat{F} | 0 \rangle$ , where  $\hat{F}$  is the pairing operator in Eq. 5. We express the function  $F(\mathbf{r}, \mathbf{r}')$  in the orbital basis, and we resolve it in terms of even and odd components,  $F_{ee}$ ,  $F_{eo}$ ,  $F_{oe}$ , and  $F_{oo}$ , as in Eq. 8.

From their translational properties, one can easily show that they all depend on the vector  $\mathbf{r}' - \mathbf{r}$  connecting the electron pair, and they are periodic functions (with periodicity set by the lattice vectors) of the pair center  $\mathbf{R}_{\text{center}}$ . The dependence on  $\mathbf{R}_{\text{center}}$  gives rise to an inhomogeneous contribution within the unit cell, while the  $\mathbf{r}' - \mathbf{r}$  dependence is set by the symmetry transformations under the 2D lattice point-group operations.

Therefore, their orbital-summed Fourier decomposition can be written in general as

$$F(\mathbf{r}, \mathbf{r}') = \sum_{\mathbf{k}, \mathbf{G}, \mathbf{G}'} F(\mathbf{k}, \mathbf{G}, \mathbf{G}') e^{i\mathbf{k} \cdot (\mathbf{r}' - \mathbf{r})} e^{-i\mathbf{G} \cdot \mathbf{r}} e^{-i\mathbf{G}' \cdot \mathbf{r}'}, \quad (31)$$

where  $\mathbf{k}$  leaves in the 2D Brillouin zone of the iron lattice plane, and  $\mathbf{G}$  and  $\mathbf{G}'$  are reciprocal lattice vectors of the 3D Bravais lattice of the crystal.

From Eq. 31, their parity-resolved Fourier components are analytically given by

$$F_{pp'}(\mathbf{k}, \mathbf{G}, \mathbf{G}') = \sum_{\substack{\{\nu\} \in p \\ \{\mu\} \in p'}} f(\mathbf{k})_{\nu,\mu} d_{\mathbf{k},\nu}(\mathbf{G}) d_{-\mathbf{k},\mu}(\mathbf{G}'), \quad (32)$$

where  $p$  ( $p'$ ) is the parity under reflection through the iron plane of the left (right) orbital, and  $d_{\mathbf{k},\nu}(\mathbf{G})$  is the Fourier

component of the  $\nu$  orbital evaluated at the  $\mathbf{k} + \mathbf{G}$  reciprocal vector in the gauge representation, corresponding to the  $d_{\mathbf{k}+\mathbf{Q},\nu}(\mathbf{G})$  component in the “physical” representation. Eq. 32 can be evaluated on a dense k-point grid thanks to the BCS interpolation  $f^{BCS}(\mathbf{k})_{\nu,\mu}$  of the QMC pairing function. In the following we compute Eq. 32 by taking  $f^{BCS}(\mathbf{k})_{\nu,\mu}$  and the Fourier components of the periodic Gaussian d-orbital with exponent  $Z = 0.8$ .

Within the “improper s-wave” picture,  $F_{pp'}(\mathbf{k}, \mathbf{G}, \mathbf{G}')$  have the following properties, according to the z-component values of  $\mathbf{G}$  and  $\mathbf{G}'$ :

- For  $G_z = 0$  and  $G'_z = 0$ , the only non-zero components are of type “even-even”, they are purely real, and they have a standard s-wave symmetry, as seen in Fig. 8(a);
- For  $G_z \neq 0$ , or  $G'_z \neq 0$ , the improper symmetry shows up in the “even-odd” and “odd-even” components, which are purely imaginary, and they have a  $d_{xy}$ -wave symmetry (see, for instance, Fig. 8(b));
- All the other “even-even” and “odd-odd” components are purely real and of s-wave symmetry (see Figs. 8(c) and 8(d)).

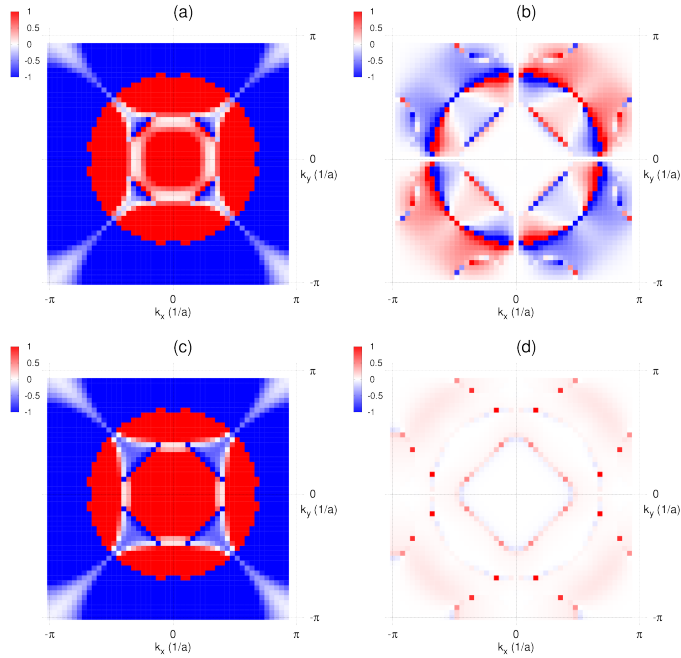


FIG. 8: Fourier components of the pairing function on a  $50 \times 50$  k-point grid in the unfolded Brillouin zone. Panel (a): even-even  $G_z = 0$   $G'_z = 0$  component; Panel (b): even-odd (equal to odd-even by symmetry)  $G_z = \frac{2\pi}{c}$   $G'_z = \frac{2\pi}{c}$  component; Panel (c): even-even  $G_z = \frac{2\pi}{c}$   $G'_z = \frac{2\pi}{c}$ ; Panel (d): odd-odd  $G_z = \frac{2\pi}{c}$   $G'_z = \frac{2\pi}{c}$ .

## V. PHYSICAL CONSEQUENCES OF THE IMPROPER S-WAVE SYMMETRY

We explore now the physical consequences of the improper s-wave from a general perspective, by assuming that also the other IBS families have a  $A_{1g}$  superconducting gap, as the FeSe. First of all, the twofold symmetry of the pairing function observed by STM<sup>16</sup> in stoichiometric FeSe with impurities and magnetic field can be explained by the Andreev resonance probed by the STM and sensitive to the sign change induced by a planar superposition of the s- and d-wave channels, invariant under  $\pi$  rotations. Note that the  $d_{xy}$  arrangement is in agreement with the different orientations measured by the STM zero bias conductance. In Fig. 9, by plotting the QMC pairing function at different distances from the iron plane, we show how the  $C_4$  is broken as soon as the experimental local probe is lifted from the iron layer.

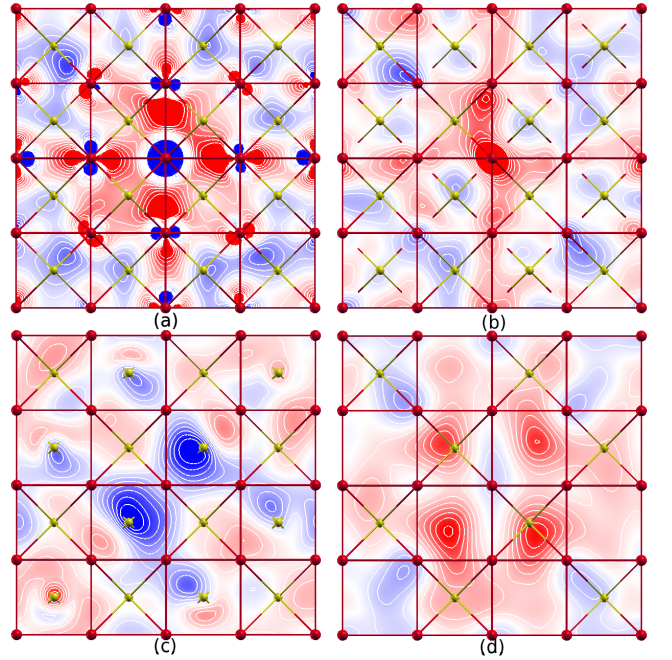


FIG. 9: Contour plot of the total QMC pairing function projected on a plane at different heights in the unit cell. (a) is at  $z = 0$  which coincides with the iron plane, (b) is at  $z = 0.125c$ , (c) is at  $z = 0.25c$ , and finally (d) is at  $z = 0.5c$ .

From ab-initio DFT and DMFT calculations,<sup>18,19</sup> the  $d_{x^2-y^2}$  and  $d_{3z^2-r^2}$  orbitals are usually pseudogapped. This allows us to disregard them from the summation in Eq. 5. Thus,  $d_{xy}$  is the only remaining orbital with even parity, and it can trigger the formation of the d-wave channel in the pairing function. Indeed, for absent or weak  $d_{xy}$  spectral weight at the Fermi level, the two orbitals left in  $F$  are both odd under  $\sigma_h$ , and therefore they can only contribute to the s-wave channel.

In the “111” family, DFT band structure calculations and de Haas-van Alphen experiments show that the main effect of P isovalent substitution is the formation of the third hole pocket - with dominant  $d_{xy}$  character -, absent in the LiFeAs.<sup>46</sup> The enhanced  $d_{xy}$  spectral weight in the P substituted compound

and the subsequent development of an “even-odd” d-wave pairing gap can explain why the LiFeP pairing is nodal, while the LiFeAs shows a fully gapped behavior.

Within the improper s-wave picture, the properties of the “1111” family modified by impurity substitution as in Ref. 14 are consistent with a tendency of  $F$  to develop nodes by going from Co to Mn doping through the opening of the d-wave channel. Indeed, Co impurities are electron donors, while Mn impurities dope the system with hole, thus enhancing the  $d_{xy}$  spectral weight around  $\Gamma$ .

The “122” family does not belong to the  $P4/nmm$  space-group. Nevertheless, by inspection of its  $I4/mmm$  space-group unit cell, one can see that also in that case the  $S_4$  improper rotation is the valid symmetry on the iron layer, thus the improper s-wave theory applies also here. The  $s$ -to- $d$  wave transition by doping the  $\text{BaFe}_2\text{As}_2$  with K is one of the most striking experimental situations for us.<sup>12</sup> In the strong overdoped regime, the band structure certainly shows all three pockets at  $\Gamma$  with again an enhanced  $d_{xy}$  spectral weight. If the d-wave channel dominates in the improper s-wave gap, then it is plausible that the experimental thermodynamic features are compatible with a pure d-wave behavior.

Finally, we would like to point out that the importance of the third hole pocket, with strong  $d_{xy}$  character, has already been observed by Kuroki and co-workers in relation to the  $T_c$  dependence on the pnictogen height.<sup>47</sup> The improper s-wave symmetry explains the key role played by  $d_{xy}$ , particularly in connection with the appearance of gap nodes, the twofold anisotropy, and the stabilization of the d-wave channel, by rec-

onciling a series of experiments which look otherwise contradictory. It suggests also that the pnictogen or the chalcogen, rather than being spectators, take an active role in the electronic pairing, by bridging two next-nearest neighbor iron sites in a  $d_{xy}$  fashion via the improper s-wave symmetry.

From the theoretical point of view, there is a lot of confusion in literature. For instance, to our knowledge, no RPA and no mean-field studies have been done so far with a low energy 2D model explicitly compatible with the improper rotations and gauged translation invariance. As we have shown translation invariance and  $C_{4v}$  have to be combined in an appropriate way, by taking particular attention to the even/odd  $\sigma_h$  reflection of the orbitals in the model. In our QMC simulations the improper s-wave symmetry is stabilized, which determines a highly entangled nodal structure of the pairing function, and the possibility for mixing between s-wave and d-wave components, an effect that, as we discussed, is crucial to understand most experiments in the iron-based superconductors.

### Acknowledgments

We acknowledge useful discussions with S. Biermann, T. Cren, M. Fabrizio, A. Savin, and D. J. Scalapino. The HPC resources have been provided under the IDRIS/GENCI 2012096493 and CINECA-MIUR ISCRA-HP10A2GZHV grants.

\* michele.casula@impmc.upmc.fr

† sorella@sissa.it

<sup>1</sup> J. Paglione, and R. L. Greene, Nature Phys. **6**, 645 (2010).

<sup>2</sup> In the following, for simplicity of notations, we identify the subgroup symbols  $S_4$  or  $C_4$  with the elementary operation (e.g. rotation by  $\pi/2$ ) that defines the cyclic subgroup.

<sup>3</sup> G. R. Stewart, Rev. Mod. Phys. **83**, 1589 (2011).

<sup>4</sup> P. J. Hirschfeld, M. M. Korshunov, and I. I. Mazin, Rep. Prog. Phys. **74** 124508 (2011).

<sup>5</sup> I. I. Mazin, D. J. Singh, M. D. Johannes, and M. H. Du, Phys. Rev. Lett. **101**, 057003 (2008).

<sup>6</sup> K. Kuroki, S. Onari, R. Arita, H. Usui, Y. Tanaka, H. Kontani, and H. Aoki, Phys. Rev. Lett. **101**, 087004 (2008).

<sup>7</sup> S. Graser, A. F. Kemper, T. A. Maier, H. P. Cheng, P. J. Hirschfeld, and D. J. Scalapino, Phys. Rev. B **81**, 214503 (2010).

<sup>8</sup> K. Suzuki, H. Usui, and K. Kuroki, J.Phys.Soc.Japan **80**, 013710 (2011).

<sup>9</sup> I. I. Mazin, T. P. Devereaux, J. G. Analytis, J.-H. Chu, I. R. Fisher, B. Muschler, and R. Hackl, Phys. Rev. B **82**, 180502(R) (2010).

<sup>10</sup> F. Ning, K. Ahilan, T. Imai, A. S. Sefat, R. Jin, M. A. McGuire, B. C. Sales, and D. Mandrus, J. Phys. Soc. Japan **77**, 103705 (2008).

<sup>11</sup> K. Hashimoto, S. Kasahara, R. Katsumata, Y. Mizukami, M. Yamashita, H. Ikeda, T. Terashima, A. Carrington, Y. Matsuda, T. Shibauchi, Phys. Rev. Lett. **108**, 047003 (2012).

<sup>12</sup> J-Ph. Reid, A. Juneau-Fecteau, R. T. Gordon, S. René de Cotret, N. Doiron-Leyraud, X. G. Luo, H. Shakeripour, J. Chang, M. A. Tanatar, H. Kim, R. Prozorov, T. Saito, H. Fukazawa, Y. Kohori, K. Kihou, C. H. Lee, A. Iyo, H. Eisaki, B. Shen, H.-H. Wen, and

L. Taillefer, Supercond. Sci. Technol. **25**, 084013 (2012).

<sup>13</sup> J. K. Dong, S. Y. Zhou, T. Y. Guan, H. Zhang, Y. F. Dai, X. Qiu, X. F. Wang, Y. He, X. H. Chen, S. Y. Li, Phys. Rev. Lett. **104**, 087005 (2010).

<sup>14</sup> M. Sato, Y. Kobayashi, S. C. Lee, H. Takahashi, E. Satomi, and Y. Miura J. Phys. Soc. Jap. **79**, 014710 (2010).

<sup>15</sup> B. Zeng, G. Mu, H. Q. Luo, T. Xiang, I. I. Mazin, H. Yang, L. Shan, C. Ren, P. C. Dai, H.-H. Wen, Nature Communications **1**, 112 (2010).

<sup>16</sup> C.-L. Song, Y.-L. Wang, P. Cheng, Y.-P. Jiang, W. Li, T. Zhang, Z. Li, K. He, L. Wang, J.-F. Jia, H.-H. Hung, C. Wu, X. Ma, X. Chen, Q.-K. Xue, Science **332**, 1410 (2011).

<sup>17</sup> D. J. Singh and M.-H. Du, Phys. Rev. Lett. **100**, 237003 (2008).

<sup>18</sup> M. Aichhorn, S. Biermann, T. Miyake, A. Georges, and M. Imada, Phys. Rev. B **82**, 064504 (2010).

<sup>19</sup> Ph. Werner, M. Casula, T. Miyake, F. Aryasetiawan, A. J. Millis, and S. Biermann, Nature Physics **8**, 331 (2012).

<sup>20</sup> S. Graser, T. A. Maier, P. J. Hirschfeld, and D. J. Scalapino, New J. Phys. **11**, 025016 (2009).

<sup>21</sup> K. Nakamura, R. Arita, and M. Imada, J. Phys. Soc. Jpn. **77**, 093711 (2008).

<sup>22</sup> T. Miyake, K. Nakamura, R. Arita, and M. Imada, J. Phys. Soc. Jpn. **79**, 044705 (2010).

<sup>23</sup> Strictly speaking, the  $d$  orbitals are zero at the iron sites. The amplitude of the pairing function is computed by integrating those orbitals over a planar mesh ( $+\delta_x, -\delta_x, +\delta_y, -\delta_y$ , with  $|\delta| = 0.25$  Bohr) around the iron center. The sign of the integrand on the mesh selects their angular symmetry.

- <sup>24</sup> R. S. Kumar, Y. Zhang, S. Sinogeikin, Y. Xiao, S. Kumar, P. Chow, A. L. Cornelius, and C. Chen, *J. Phys. Chem. B* **114**, 12597 (2010).
- <sup>25</sup> S. Margadonna, Y. Takabayashi, Y. Ohishi, Y. Mizuguchi, Y. Takano, T. Kagayama, T. Nakagawa, M. Takata, and K. Prassides, *Phys. Rev. B* **80**, 064506 (2009).
- <sup>26</sup> M. Burkatzki, Claudia Filippi, and M. Dolg, *J. Chem. Phys.* **129**, 164115 (2008).
- <sup>27</sup> J.R. Trail and R.J. Needs, *J. Chem. Phys.* **122**, 174109 (2005); J.R. Trail and R.J. Needs, *J. Chem. Phys.* **122**, 014112 (2005), see also [www.tcm.phy.cam.ac.uk/~mdt26/casino2\\_pseudopotentials.html](http://www.tcm.phy.cam.ac.uk/~mdt26/casino2_pseudopotentials.html).
- <sup>28</sup> S. Sorella, G. Martins, F. Becca, C. Gazza, L. Capriotti, A. Parola and E. Dagotto, *Phys. Rev. Lett.* **88**, 117002 (2002).
- <sup>29</sup> M. Capello, F. Becca, M. Fabrizio, S. Sorella, and E. Tosatti, *Phys. Rev. Lett.* **94**, 026406 (2005).
- <sup>30</sup> Wen-Jun Hu, Federico Becca, and Sandro Sorella *Phys. Rev. B* **85**, 081110 (2012).
- <sup>31</sup> M. Casula, C. Attacalite, and S. Sorella, *J. Chem. Phys.* **121** 7110 (2004).
- <sup>32</sup> S. Sorella, M. Casula, and D. Rocca, *J. Chem. Phys.* **127**, 014105 (2007).
- <sup>33</sup> F. Sterpone, L. Spanu, L. Ferraro, S. Sorella, L. Guidoni, *J. Chem. Theory Comput.* **4**, 1428 (2008).
- <sup>34</sup> Leonardo Spanu, Massimo Lugas, Federico Becca, and Sandro Sorella, *Phys. Rev. B* **77**, 024510 (2008).
- <sup>35</sup> Federico Becca, Luca Capriotti, Alberto Parola, and Sandro Sorella *Phys. Rev. B* **76**, 060401 (2007).
- <sup>36</sup> The LDA-DFT calculations have been performed with the Quantum-espresso<sup>37</sup> code. Fe and Se atoms are described respectively by ultrasoft (with 16 valence electrons) and norm-conserving (with 6 valence electrons) pseudopotentials generated with a scalar-relativistic calculation. The plane-wave (PW) cut-off is 60 Ry for the wave-function, and 240 Ry for the charge. A  $4 \times 4 \times 4$  electron-momentum grid and a Methfessel-Paxton smearing of 0.01 Ry are used in the electronic integration. Wannierization has been performed with the Wannier90<sup>38</sup> program on a  $N_w = 4 \times 4 \times 4$  electron-momentum mesh, by including the d states on the two inequivalent Fe site of the unit cell. The localized orbitals yield Wannierized bands in a very good agreement with those computed in the PW basis set in a window of  $\pm 1.5$  eV around the Fermi level.
- <sup>37</sup> P. Giannozzi *et al.*, *J. Phys.: Condens. Matter* **21**, 395502 (2009).
- <sup>38</sup> A. A. Mosto, J. R. Yates, Y.-S. Lee, I. Souza, D. Vanderbilt and N. Marzari, *Comput. Phys. Commun.*, **178**, 685 (2008).
- <sup>39</sup> Sandro Sorella, Michele Casula, Leonardo Spanu, and Andrea Dal Corso, *Phys. Rev. B* **83**, 075119 (2011).
- <sup>40</sup> M. Marchi, S. Azadi, S. Sorella, *Phys. Rev. Lett.* **107**, 086807 (2011).
- <sup>41</sup> S. Azadi, C. Cavazzoni and S. Sorella *Phys. Rev. B* **82**, 125112 (2010).
- <sup>42</sup> C. J. Umrigar, J. Toulouse, C. Filippi, S. Sorella, and R. G. Hennig, *Phys. Rev. Lett.* **98**, 110201 (2007).
- <sup>43</sup> M. Marchi, S. Azadi, M. Casula, S. Sorella, *J. Chem. Phys.* **131**, 154116 (2009).
- <sup>44</sup> The parity projection has been made by averaging the orbitals at opposite positions above and below the iron layer at a given distance  $\delta_z$  from it (0.25 Bohr). The odd orbitals are strictly zero at the iron layer. However, the pairing function is 3D. Averaging those orbitals above and below the layer gives a finite contribution. Therefore, the even and odd MO orbitals entering the pairing function  $\phi$  in Eq. 15 read as:
- $$\psi_i^{MO\text{ odd}}(\mathbf{r}) = 1/2(\psi_i^{MO}(\mathbf{r} + \delta_z) - \psi_i^{MO}(\mathbf{r} - \delta_z)),$$
- $$\psi_i^{MO\text{ even}}(\mathbf{r}) = 1/2(\psi_i^{MO}(\mathbf{r} + \delta_z) + \psi_i^{MO}(\mathbf{r} - \delta_z)).$$
- <sup>45</sup> At ambient pressure, the slightly broken low temperature phase is very close to the tetragonal parent structure, and their difference (around 0.01 Å between the  $a$  and  $b$  axes) has been neglected in our calculations. At 4 GPa, the  $a/b$  anisotropy is instead more than four times stronger, and thus we used the corresponding experimental low temperature orthorhombic structure.
- <sup>46</sup> C. Putzke, A. I. Coldea, I. Guillamn, D. Vignolles, A. McCollam, D. LeBoeuf, M. D. Watson, I. I. Mazin, S. Kasahara, T. Terashima, T. Shibauchi, Y. Matsuda, and A. Carrington, *Phys. Rev. Lett.* **108**, 047002 (2012).
- <sup>47</sup> K. Kuroki, H. Usui, S. Onari, R. Arita, and H. Aoki, *Phys. Rev. B* **79**, 224511 (2009).
- <sup>48</sup> J. Hu and N. Hao *Phys. Rev. X* **2**, 021009 (2012).
- <sup>49</sup> C.H. Lin, T. Berlijn, L. Wang, C. C. Lee, W.G. Yin, and W. Ku *Phys. Rev. Lett.* **107**, 257001 (2011).